ChemComm

COMMUNICATION

View Article Online
View Journal | View Issue

Cite this: *Chem. Commun.*, 2019, 55, 10693

Received 11th July 2019,
Accepted 6th August 2019

DOI: 10.1039/c9cc05322k

rsc.li/chemcomm

Direct probing of heterogeneity for adsorption and diffusion within a SAPO-34 crystal†

Shushu Gao,[ab] Shutao Xu,*[a] Yingxu Wei,*[a] Zhiqiang Liu,[c] Anmin Zheng,[cd] Pengfei Wu[a] and Zhongmin Liu*[ae]

The inhomogeneous phenomenon with a gradient distribution in adsorption and diffusion behaviors of xenon within a large SAPO-34 crystal was revealed by ^{129}Xe NMR, 2D EXSY NMR and ^{129}Xe PFG NMR techniques at the micro-scale. A multi-layer adsorption and diffusion model for xenon in a single crystal was proposed.

Spatiotemporal inhomogeneity is ubiquitous in heterogeneous catalytic processes catalyzed by nanoporous materials at the macroscopic and microscopic levels.[1,2] In zeolite-catalyzed processes, the heterogeneity in the catalyst particles is mainly dependent on the adsorption and diffusion of reactants and products within confined environments of nanopores.[1,3] The presence of diffusion limitation caused by pore architecture,[3,4] chemical composition[5] and particle size[6] results in incomplete utilization of active sites and induces the spatial and temporal heterogeneous distribution for catalytic conversion at the single crystal level. The significant role played by mass transport limitation in the heterogeneity of catalyst particles has also been confirmed in a SAPO-34 molecular sieve, a core commercial catalyst used in the methanol-to-olefin (MTO) process which is one of the most important heterogeneous catalytic reactions for the generation of light alkenes on the basis of non-oil feedstock of coal or natural gas.[7,8] SAPO-34 with chabazite (CHA) topology, consisting of CHA cages interconnected by eight-membered ring (8-MR) windows, provides a highly selective and spatially confined surrounding for adsorption, diffusion and reaction. It has been revealed that the inhomogeneous location of coke formation on individual micron-sized SAPO-34 can be attributed to the stronger diffusion resistance originating from outer pore blockage by coke which prevents reactants from contacting inner active sites during the MTO reaction.[3,9] However, a direct investigation of adsorption and mass transport in catalyst particles and the corresponding contributions to inhomogeneous coke formation is still scarce and required to be solved as an essential issue.[10] Consequently, a further fundamental insight into adsorption and diffusion behaviors is extremely indispensable for achieving the in-depth understanding of the role of adsorption and mass transport in catalytic processes, and may provide new insights for catalyst optimization.

As a sensitive and inert probe, xenon with van der Waals diameter (4.4 Å)[11] was selected due to its suitable size that is similar to that of the 8-MR window, and the particular use of ^{129}Xe NMR. ^{129}Xe NMR is a very sensitive tool to probe the variation in the local chemical environments of nanoporous media.[12–14] Furthermore, ^{129}Xe NMR, two-dimensional (2D) exchange spectroscopy (EXSY) NMR and pulsed field gradient (PFG) NMR techniques were used to explore the adsorption and diffusion processes within the pores of the SAPO-34 molecular sieve based on the host–guest interactions. This work proved that the heterogeneities in adsorption and diffusion behaviors of xenon, featuring a gradient distribution, exist in the SAPO-34 molecular sieve on a single crystal scale.

The physicochemical properties of the as-synthesized SAPO-34 molecular sieve are presented in the ESI.† The XRD and SEM results show that SAPO-34 is a high-crystalline cubic crystal with a crystallite size of *ca.* 15 μm (Fig. S1 and S2, ESI†). The SAPO-34 molecular sieve with different xenon loadings was prepared (see details in the ESI†). ^{129}Xe NMR spectra of SAPO-34 are displayed in Fig. 1a, recorded at a series of average xenon loadings from 0.1 to 3.6 xenon atoms per cage at 298 K. The NMR signals at higher field are assigned to gaseous xenon. And the broad peaks at lower field in the spectra originate from xenon adsorbed inside the CHA cages of SAPO-34.[15,16] It is well known that the chemical

[a] *National Engineering Laboratory for Methanol to Olefins, Dalian National Laboratory for Clean Energy, iChEM (Collaborative Innovation Center of Chemistry for Energy Materials), Dalian Institute of Chemical Physics, Chinese Academy of Sciences, Dalian 116023, P. R. China. E-mail: xushutao@dicp.ac.cn, weiyx@dicp.ac.cn, liuzm@dicp.ac.cn*
[b] *University of Chinese Academy of Sciences, Beijing 100049, P. R. China*
[c] *State Key Laboratory of Magnetic Resonance and Atomic and Molecular Physics, National Center for Magnetic Resonance in Wuhan, Wuhan Institute of Physics and Mathematics, Chinese Academy of Sciences, Wuhan 430071, P. R. China*
[d] *School of Materials Science and Engineering, Zhengzhou University, Zhengzhou 450001, P. R. China*
[e] *State Key Laboratory of Catalysis, Dalian Institute of Chemical Physics, Chinese Academy of Sciences, Dalian 116023, P. R. China*

† Electronic supplementary information (ESI) available. See DOI: 10.1039/c9cc05322k

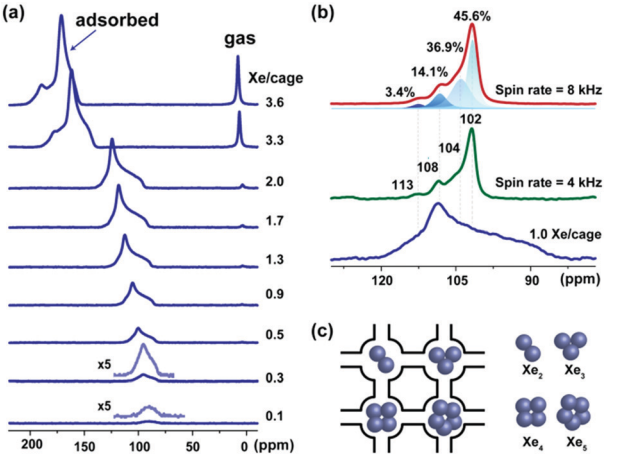

Fig. 1 (a) Loading-dependent ^{129}Xe NMR spectra of xenon adsorbed in the SAPO-34 molecular sieve at 298 K under static conditions. (b) ^{129}Xe MAS NMR spectra at a spinning rate of 8 kHz and 4 kHz and the corresponding static spectra of xenon adsorbed in SAPO-34 with an average loading of one atom per cage at 298 K. The fitting peaks are shown as color-filled from light to dark blue. (c) Possible local structure of Xe_n clusters inside the CHA cages of SAPO-34.

shift (δ) of xenon depends on different interactions and can be summarized by the expression:[16] $\delta = \delta_0 + \delta_S + \delta_{Xe\text{–}Xe} + \delta_{SAS} + \delta_E + \delta_M$. Here, δ_0 is set to 0 ppm (the chemical shift of xenon at zero pressure). δ_s denotes xenon–surface interactions (depending on the dimension and shape of the channel or cavity). δ_{SAS} characterizes the interactions between xenon and strong adsorption sites. $\delta_{Xe\text{–}Xe}$ arises from xenon–xenon interactions and is related to xenon density. δ_E and δ_M arise from the contribution of electrostatic field and magnetic field by cations, respectively. For the H-SAPO-34 molecular sieve, the contributions from δ_{SAS}, δ_E and δ_M can be neglected,[11,17] then the chemical shift δ can be briefly written as $\delta = \delta_0 + \delta_S + \delta_{Xe\text{–}Xe}$.

As shown in Fig. 1a, the increased chemical shift of the adsorbed xenon indicates that more xenon atoms occupy the confined space of cages which leads to increased xenon–xenon interactions.[11,16] An obvious asymmetric line shape and large line width for the adsorbed xenon are also observed in the NMR spectra as xenon loading increases. Such loading-dependent line shape for the adsorbed xenon may arise from various Xe_n clusters (n denotes the number of xenon atoms) within the confined space or can be attributed to chemical shift anisotropic (CSA) line shape, because all ^{129}Xe NMR spectra were obtained under static conditions. This line shape is further verified by the fact that the NMR line shape remains unchanged when increasing the equilibration time to 3 months at 298 K (see Fig. S3, ESI†). As a result, the dynamic equilibrium has been established in the host–guest system at the macro-scale.

To clarify the above case, the ^{129}Xe magic angle spinning (MAS) NMR experiment was performed (see details in the ESI†). The chemical shift anisotropy of the adsorbed xenon is effectively averaged by fast magic angle spinning of 4 and 8 kHz (Fig. 1b), however, multiple signals of the adsorbed xenon within cavities still exist. This indicates that inhomogeneous distribution of xenon inside SAPO-34 occurs. Furthermore, by fitting the ^{129}Xe MAS NMR spectrum (Fig. 1b) with Dmfit software,[17] four isotropic resonance signals at 113, 108, 104 and 102 ppm were plotted (color-filled). The fitting separate lines of the adsorbed xenon in SAPO-34 should be directly related to different xenon–xenon interactions, corresponding to different Xe_n clusters with different atoms inside CHA cavities. Therefore, ^{129}Xe MAS NMR spectra shed light on the existence of at least four types of Xe_n clusters inside cavities and imply that the asymmetric line shape of xenon adsorbed inside SAPO-34 is mainly attributed to inhomogeneous xenon distribution.

Such behavior can be related to the basic structural properties of porous materials. The existence of different Xe_n clusters has been confirmed in A-type zeolites with the 8-MR and the cavity structure, for which multiple resolved peaks were observed in ^{129}Xe NMR spectra.[18–20] This is due to diffusion limitation from narrow pore openings of zeolites for inter-cavity diffusion of xenon and xenon atoms cannot be exchanged rapidly between the different cavities. The chemical shift of Xe_n clusters increases with the number of xenon atoms. The smallest increment of the chemical shift between Xe_1 (one xenon atom per cage) and Xe_2 (two xenon atoms per cage) is about 20 ppm and the increment between Xe_n and Xe_{n-1} clusters increases with the number of xenon atoms of Xe_n clusters in Na–A zeolites.[18] However, the fast exchange among Xe_n clusters inside CaA zeolites results in a single averaged signal in ^{129}Xe NMR spectra.[20] The Xe_n cluster model is also applied in other microporous materials under fast-exchange conditions.[21]

In the case of SAPO-34, in the present work, it is reasonable to infer that the minor difference in the chemical shift between adjacent signals is probably ascribed to the faster exchange among Xe_n clusters in CHA cages compared to that in Na–A zeolites in which the 8-MR window is partially blocked by Na^+ ions. For SAPO-34, the chemical shift of one xenon atom inside the CHA cage (Xe_1) was found to be 84 ppm.[15,16] Dimension limitation of the CHA cage indicates that maximum five atoms can be loaded (see Fig. S4, ESI†), corresponding to the NMR peak with the highest chemical shift value (113 ppm). Other peaks differ in the number of xenon atoms in cages (Xe_4, Xe_3 and Xe_2) with decreasing chemical shift (Fig. 1c). For such heterogeneous xenon distribution inside the CHA cages of SAPO-34 with the average loading of one xenon atom per cage (Fig. 1b), the calculated utilization ratio (defined as the ratio of the number of occupied cages to the number of all cages in a single crystal) of 0.39 for an individual SAPO-34 crystal reveals that most of the CHA cages are empty (see Table S2, ESI†). Therefore, the information on the local structure of Xe_n clusters in CHA cages revealed by chemical shifts of ^{129}Xe reflects the important consequence for adsorption and mass transport inside a SAPO-34 crystal.

To further obtain detailed location information of these Xe_n clusters in a single SAPO-34 crystal from the micrometre-scale, 2D EXSY NMR spectroscopy was employed to provide dynamic information about the motion pathways of xenon between different sites.[22,23] The occurrence of cross peaks in the off-diagonal of spectra indicates a correlation between two sites at given mixing time, *i.e.* exchange of xenon occurs between the

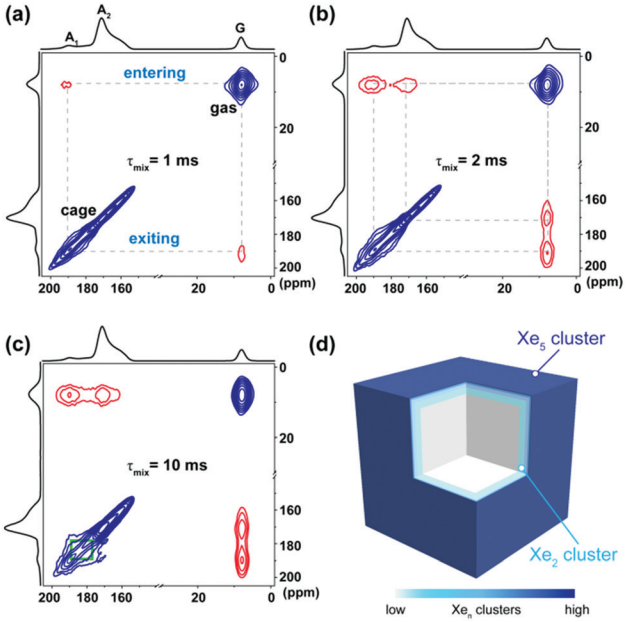

Fig. 2 2D EXSY NMR spectra of xenon adsorbed in the SAPO-34 molecular sieve with an average loading of 3.6 xenon atoms per cage at 298 K with mixing times of 1 ms (a), 2 ms (b), and 10 ms (c), respectively. The existence of cross peaks (red lines) indicates the xenon exchange between the gas phase and CHA cages of SAPO-34. The green dashed line represents the exchange between different adsorption sites in the micropores of SAPO-34. (d) Possible spatial location of Xe_n clusters in a single SAPO-34 crystal. The colors from dark to light blue represent the decrease of the number of xenon per cage with the depth from the surface to interior.

adsorbed xenon and gaseous phase. Fig. 2 displays 2D ^{129}Xe EXSY NMR spectra with increased mixing times (τ_m). The exchange between the adsorbed xenon (A) and gaseous phase (G) was unobservable and only diagonal peaks corresponding to the self-correction of the adsorbed xenon or gaseous phase were observed at a short mixing time of 0.2 ms (see Fig. S5a, ESI†). As the mixing time increases to 1 ms, xenon from the gaseous phase exchanges first with adsorbed xenon A_1 (defined as large size Xe_n clusters as revealed in Fig. 1b) inside cages, and exchanges further with adsorbed xenon A_2 (defined as small size Xe_n clusters) as indicated by the occurrence of a characteristic cross-peak between A_2 and G at a mixing time of 2 ms (Fig. 2b). Furthermore, the exchange between the adsorbed xenon (A_1 and A_2) and gaseous phase becomes pronounced as the mixing time increases to 10 ms. Meanwhile, the inter-cage motion between different adsorbed xenon (A_1 and A_2) also can be observed (Fig. 2c) at 10 ms which is much smaller than the mixing time (τ_m = 200 ms) observed in NaA zeolites at 303 K.[24] This indicates the faster exchange among Xe_n clusters in SAPO-34 compared to that in NaA, which agrees with our aforementioned inference.

This evolution feature of 2D EXSY NMR spectra with mixing time indicates the characteristic of the xenon location in crystals, and can be readily understood by considering the effect of motion pathways. Given the identical CHA cavity environments of SAPO-34 (see Fig. S6, ESI†), a faster exchange between G and A_1 than that between G and A_2 indicates that the mean distance between A_1 and G is shorter than that between A_2 and G. As a result, it is reasonable to infer that adsorbed xenon A_1 and A_2 come from the surface and inner regions of the SAPO-34 crystal, respectively, which implies that the number of atoms per cage decreases from the surface region to the inner region of the crystal, featuring a decreased size of Xe_n clusters. The relative proportion of Xe_n clusters inside the SAPO-34 crystal enhances as the chemical shift decreases as shown in Fig. 1b, indicating that the number of occupied cages loaded with different Xe_n clusters increases from the surface to the core of the crystal. Based on the above analysis, the location of Xe_n clusters in a single SAPO-34 crystal can be visualized, as modeled in Fig. 2d. Here, Table S2 (ESI†) summarizes the proportion of occupied cages from the core to surface regions and the thickness of each region in a single crystal (on the basis of an essential assumption that each region has the same Xe_n clusters and all cages are occupied in this region). Since the utilization ratio for an individual SAPO-34 crystal is smaller than 1, some CHA cages are empty. Therefore, 2D EXSY NMR provides straightforward evidence for the spatial location of different Xe_n clusters in a single SAPO-34 crystal in the micrometre-level.

Such an exchange between adsorbed and gaseous xenon at thermodynamic equilibrium actually represents the inter-cage motion, which is also the basic step for mass transport inside the SAPO-34 crystal. The presence of Xe_n clusters with a gradient distribution in a single SAPO-34 crystal is probably attributed to the surface barrier or internal diffusion resistance, originating from surface composition or internal intergrowth structures.[1,25,26] This inhomogeneous adsorption phenomenon is also influenced by crystallite size and temperature. The asymmetric line shape of the adsorbed xenon with a smaller crystallite size of 400 nm was less obvious, indicating a faster exchange among Xe_n clusters in a small crystal than in a large crystal (Fig. S7, ESI†). The line shape of the adsorbed xenon is essentially dependent on temperature (Fig. S8, ESI†). At lower temperature, the multiple resonance line of the adsorbed xenon becomes more resolved and the proportion of Xe_n also changed, which may be due to the slower exchange rate among Xe_n clusters at lower temperature.

An extensive investigation for intracrystalline diffusion dependency on xenon loading in a SAPO-34 crystal by PFG NMR was subsequently performed. Due to the presence of CSA line shape for the adsorbed xenon, diffusion dependency on the spatial location of different Xe_n clusters in the SAPO-34 crystal cannot be determined separately by PFG NMR under static conditions. ^{129}Xe PFG NMR spin echo attenuation I/I_0 decays as a function of $\delta^2\gamma^2g^2(\Delta - \delta/3)$ on a log-linear scale for xenon inside the SAPO-34 molecular sieve recorded at 298 K (see Fig. S9, ESI†). A remarkable enhancement in the average self-diffusion coefficient from 6.2×10^{-13} to 5.8×10^{-12} m^2 s^{-1} for xenon adsorbed in SAPO-34 was displayed as the average loading increased from 1.3 to 4.0 xenon atoms per cage at 298 K (Fig. 3). This clearly shows that the self-diffusion coefficient of xenon adsorbed inside SAPO-34 is strongly dependent on xenon loading. The increased intracrystalline diffusion coefficient of xenon with loading implies that the adsorbed xenon located at the near exterior surface of the crystal may exhibit a faster diffusivity due to its higher xenon loading. It is

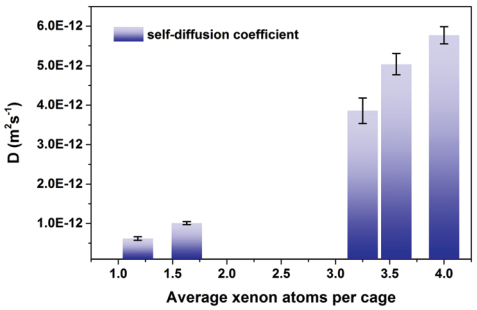

Fig. 3 Loading dependence of self-diffusion coefficients for xenon in SAPO-34 molecular sieves at 298 K. The error bars are based on the standard errors.

worth mentioning that it is difficult to obtain the self-diffusion coefficient of the adsorbed xenon with very low loading due to short transverse relaxation time (T_2, see Fig. S10, ESI†) which leads to the rapid decays of ^{129}Xe echo attenuation once the pulsed magnetic field gradients (g) are applied. Therefore, the diffusivity results also provide information about the presence of heterogeneity in the diffusion of xenon inside the SAPO-34 crystal, featuring the enhanced xenon diffusivity from the inner region to the surface region of the crystal.

In summary, the non-uniform distribution of xenon inside SAPO-34 crystals in the micro-level was revealed by multiple ^{129}Xe NMR methods. Based on ^{129}Xe MAS NMR and 2D EXSY NMR spectroscopy, the presence of different Xe_n clusters confined in cages and the corresponding adsorption regions in a single SAPO-34 crystal could be identified, featuring with the enhanced number of xenon atoms of Xe_n clusters from the inner region to the exterior surface region of the crystal. PFG NMR diffusion exhibited a faster diffusivity of xenon adsorbed at the near outer surface region of the crystal due to its high xenon loading. Knowledge of such small scale heterogeneity in zeolite-based catalysts is of great importance for revealing catalytic processes under the real reaction conditions and optimizing catalysts in heterogeneous catalysis. The observation of inhomogeneous adsorption and diffusion together with catalyst deactivation in the MTO process triggered the understanding of diffusion limitation and provided insights into the relationship between adsorption, diffusion and catalyst deactivation in the MTO reaction. Longer diffusion paths arising from large crystal size and internal diffusion resistance would cause the inhomogeneous reaction on the microporous materials, which should be considered in developing new catalysts and processes.

This work was supported by the National Natural Science Foundation of China (21473182, 91545104, 91745109, and 21422606), the LiaoNing Revitalization Talents Program (XLYC1807227), the Youth Innovation Promotion Association of the Chinese Academy of Sciences (2014165), the Key Research Program of Frontier Sciences, Chinese Academy of Sciences (QYZDY-SSW-JSC024), the International Partnership Program of Chinese Academy of Sciences (121421KYSB20180007) and the Strategic Priority Research Program of the Chinese Academy of Sciences (XDB10020202 and XDA21030200).

Conflicts of interest

There are no conflicts to declare.

References

1 B. M. Weckhuysen, *Angew. Chem., Int. Ed.*, 2009, **48**, 4910–4943.
2 I. L. C. Buurmans and B. M. Weckhuysen, *Nat. Chem.*, 2012, **4**, 873–886.
3 D. Mores, E. Stavitski, M. H. F. Kox, J. Kornatowski, U. Olsbye and B. M. Weckhuysen, *Chem. – Eur. J.*, 2008, **14**, 11320–11327.
4 L. Karwacki, M. H. F. Kox, D. A. M. de Winter, M. R. Drury, J. D. Meeldijk, E. Stavitski, W. Schmidt, M. Mertens, P. Cubillas, N. John, A. Chan, N. Kahn, S. R. Bare, M. Anderson, J. Kornatowski and B. M. Weckhuysen, *Nat. Mater.*, 2009, **8**, 959–965.
5 L. R. Aramburo, E. de Smit, B. Arstad, M. M. van Schooneveld, L. Sommer, A. Juhin, T. Yokosawa, H. W. Zandbergen, U. Olsbye, F. M. F. de Groot and B. M. Weckhuysen, *Angew. Chem., Int. Ed.*, 2012, **51**, 3616–3619.
6 W. L. Dai, G. J. Wu, L. D. Li, N. J. Guan and M. Hunger, *ACS Catal.*, 2013, **3**, 588–596.
7 I. Yarulina, A. D. Chowdhury, F. Meirer, B. M. Weckhuysen and J. Gascon, *Nat. Catal.*, 2018, **1**, 398–411.
8 P. Tian, Y. X. Wei, M. Ye and Z. M. Liu, *ACS Catal.*, 2015, **5**, 1922–1938.
9 S. S. Gao, S. T. Xu, Y. X. Wei, Q. L. Qiao, Z. C. Xu, X. Q. Wu, M. Z. Zhang, Y. L. He, S. L. Xu and Z. M. Liu, *J. Catal.*, 2018, **367**, 306–314.
10 J. C. Saint Remi, A. Lauerer, C. Chmelik, I. Vandendael, H. Terryn, G. V. Baron, J. F. M. Denayer and J. Kärger, *Nat. Mater.*, 2015, **15**, 401–406.
11 T. Ito and J. Fraissard, *J. Chem. Phys.*, 1982, **76**, 5225–5229.
12 S. Komulainen, J. Roukala, V. V. Zhivonitko, M. A. Javed, L. J. Chen, D. Holden, T. Hasell, A. Cooper, P. Lantto and V. V. Telkki, *Chem. Sci.*, 2017, **8**, 5721–5727.
13 H. C. Hoffmann, B. Assfour, F. Epperlein, N. Klein, S. Paasch, I. Senkovska, S. Kaskel, G. Seifert and E. Brunner, *J. Am. Chem. Soc.*, 2011, **133**, 8681–8690.
14 E. Weiland, M.-A. Springuel-Huet, A. Nossov and A. Gédéon, *Microporous Mesoporous Mater.*, 2016, **225**, 41–65.
15 S. T. Xu, W. P. Zhang, X. C. Liu, X. W. Han and X. H. Bao, *J. Am. Chem. Soc.*, 2009, **131**, 13722–13727.
16 J.-L. Bonardet, J. Fraissard, A. Gédéon and M.-A. Springuel-Huet, *Catal. Rev.: Sci. Eng.*, 1999, **41**, 115–225.
17 D. Massiot, F. Fayon, M. Capron, I. King, S. Le Calvé, B. Alonso, J.-O. Durand, B. Bujoli, Z. Gan and G. Hoatson, *Magn. Reson. Chem.*, 2002, **40**, 70–76.
18 C. J. Jameson, A. K. Jameson, R. Gerald and A. C. de Dios, *J. Chem. Phys.*, 1992, **96**, 1676–1689.
19 B. F. Chmelka, D. Raftery, A. V. McCormick, L. C. de Menorval, R. D. Levine and A. Pines, *Phys. Rev. Lett.*, 1991, **66**, 580–583.
20 C. J. Jameson, A. K. Jameson, R. Gerald and A. C. de Dios, *J. Chem. Phys.*, 1992, **96**, 1690–1697.
21 H. Omi, T. Ueda, N. Kato, K. Miyakubo and T. Eguchi, *Phys. Chem. Chem. Phys.*, 2006, **8**, 3857–3866.
22 C. L. Perrin and T. J. Dwyer, *Chem. Rev.*, 1990, **90**, 935–967.
23 A. Comotti, S. Bracco, P. Valsesia, L. Ferretti and P. Sozzani, *J. Am. Chem. Soc.*, 2007, **129**, 8566–8576.
24 R. G. Larsen, J. Shore, K. Schmidt-Rohr, L. Emsley, H. Long, A. Pines, M. Janicke and B. F. Chmelka, *Chem. Phys. Lett.*, 1993, **214**, 220–226.
25 L. Karwacki, E. Stavitski, M. H. F. Kox, J. Kornatowski and B. M. Weckhuysen, *Angew. Chem., Int. Ed.*, 2007, **46**, 7228–7231.
26 M. B. Gao, H. Li, M. Yang, S. S. Gao, P. F. Wu, P. Tian, S. T. Xu, M. Ye and Z. M. Liu, *Chem. Commun*, 2019, **2**, 43–53.

